Dose estimation and shielding calculation for X-ray hazard at high intensity laser facilities *

QIU Rui(邱睿)[1,2,3] ZHANG Hui(张辉)[1,2,3] YANG Bo(杨博)[1,2,3] James C. Liu[4]
Sayed H. Rokni[4] Michael B. Woods[4] LI Jun-Li(李君利)[1,2,3;1)]

[1] Department of Engineering Physics, Tsinghua University, Beijing 100084, China
[2] Key Laboratory of High Energy Radiation Imaging Fundamental Science, Beijing 100084, China
[3] Key Laboratory of Particle & Radiation Imaging of Ministry of Education, Beijing 100084, China
[4] SLAC National Accelerator Laboratory: 2575 Sand Hill Road, Menlo Park, CA, 94025, USA

Abstract: An ionizing radiation hazard produced from the interaction between high intensity lasers and solid targets has been observed. Laser-plasma interactions create "hot" electrons, which generate bremsstrahlung X-rays when they interact with ions in the target. However, up to now only limited studies have been conducted on this laser-induced radiological protection issue. In this paper, the physical process and characteristics of the interaction between high intensity lasers and solid targets are analyzed. The parameters of the radiation sources are discussed, including the energy conversion efficiency from laser to hot electrons, hot electron energy spectrum and electron temperature, and the bremsstrahlung X-ray energy spectrum produced by hot electrons. Based on this information, the X-ray dose generated with high-Z targets for laser intensities between 10^{14} and 10^{20} W/cm^2 is estimated. The shielding effects of common shielding items such as the glass view port, aluminum chamber wall and concrete wall are also studied using the FLUKA Monte Carlo code. This study provides a reference for the dose estimation and the shielding design of high intensity laser facilities.

Key words: X-ray, high intensity laser, dose, shielding, Monte Carlo

PACS: 52.38.Ph, 87.53.Bn, 28.41.Qb **DOI:** 10.1088/1674-1137/38/12/129001

1 Introduction

With the rapid development of laser technology, a number of high intensity laser devices are emerging around the world. At the same time, an ionizing radiation hazard produced from the interaction between high intensity lasers and solid targets has gradually been observed.

A plasma is produced when a pulsed laser beam is focused on a solid target at peak intensities of 10^{12} W/cm^2 or higher [1]. Laser-plasma interactions subsequently accelerate electrons to high energies (10's to 1000's of keV), thereby creating "hot" electrons. These hot electrons have a Maxwellian-like energy distribution characterized by an electron temperature. The hot electrons interact with ions in the target and generate bremsstrahlung X-rays, which become an ionizing radiation source [2–6].

Measurements show that significant amounts of radiation can be generated from this ionizing radiation source at high intensity laser facilities [5, 6]. R. J. Clarke et al. measured photon doses of up to 43 mSv at 1 m per shot at a laser intensity of $\sim 4\times10^{20}$ W/cm^2 with $\sim$230 J on a 1 mm thick gold target in the Vulcan petawatt laser system at the CCLRC Rutherford Appleton Laboratory [6]. F Borne et al. reported that gamma dose equivalents in the vicinity of the chamber varied between 0.7 and 73 mSv at a laser intensity of 10^{19} W/cm^2 for 150 laser shots (300 femtoseconds) with energies in the 1 to 20 J range on solid targets such as Teflon and Au [5].

Therefore, it is necessary to analyze, evaluate and mitigate the X-ray hazard when a high intensity laser is hitting a target in a vacuum. However, very limited studies have been performed on laser-induced ionizing radiation hazards and related protection issues.

In 2006, Y. Hayashi et al. proposed an equation which can estimate the photon dose generated by the laser interaction with a solid target. This equation establishes the relationship between the photon dose and two physical parameters related to hot electrons: the

Received 9 December 2013, Revised 7 July 2014
∗ Supported by National Natural Science Foundation of China (11105081, 11275110, 11375103)
1) E-mail: lijunli@mail.tsinghua.edu.cn

electron temperature and the laser-to-electron energy conversion efficiency [7]. For the shielding design and radiation safety system of laser facilities, few studies have been reported.

In this paper, there is an extensive review of the existing literature on the physics and characteristics of hot electrons and laser-induced X-rays. Based on this information, the relationship between the photon dose and the laser intensity is established, which is more useful in practice. The photon dose due to the laser-target interaction is then estimated for laser systems with different laser intensities. In order to provide some reference for the shielding design of laser facilities, the shielding effects of common shielding items such as the glass view port, aluminum chamber wall and concrete wall were studied using the Monte Carlo code FLUKA.

2 Source term and characteristics

As mentioned above, bremsstrahlung X-rays are generated by hot electrons, which are accelerated due to the laser-plasma interactions. In order to estimate the X-ray dose and carry out radiation protection studies, it is first necessary to understand the physical characteristics of the hot electrons. The most important aspects include the yield, the energy distribution and the angular distribution of the hot electrons.

Three key factors which describe the electron source term are discussed in the following sections: i) the laser-to-electron energy conversion efficiency, ii) the electron spectrum and electron temperature, and iii) the angular distribution of the hot electrons.

2.1 Laser-to-electron energy conversion efficiency

The electron yield is characterized by the laser-to-electron energy conversion efficiency, which represents the fraction of the laser energy on the target converted to the total energy of hot electrons. Many experiments show that 10%–50% of laser energy is converted to hot electrons at incident intensities of 10^{18} to 10^{20} W/cm^2 [8, 9], though the data are not always conclusive and consistent. Ref. [10] gives estimations of conversion efficiencies of 12%, 18% and 50% at 2×10^{18}, 10^{19} and 3×10^{20} W/cm^2, respectively, from solid targets. On the other hand, T. Guo [2] reports that the laser-to-electron energy conversion efficiency is approximately 30% for laser intensities between 5×10^{17} and 5×10^{18} W/cm^2. A laser-to-electron energy conversion efficiency of 33% was used in the dose and shielding calculation for the National Ignition Facility [11]. In this study, a conservative conversion efficiency of 30% for laser intensity below 10^{19} W/cm^2 and 50% above 10^{19} W/cm^2 was used for absolute dose calculations (see Section 3).

2.2 Electron spectrum and electron temperature

Three slightly different distributions (Boltzmann distribution [12], Maxwellian distribution [13], and Relativistic Maxwellian distribution [5, 14]) have been used to describe the hot electron spectrum generated from a high intensity laser hitting a solid target. Whichever formula is used, the exponentially decreasing feature is well known and an effective electron temperature, T, is the key parameter to characterize the exponentially decreasing slope of the electron spectrum. The electron spectrum studies at the Lawrence Livermore National Laboratory (LLNL) [15] show that the hot electron temperature depends strongly on the laser intensity and wavelength but not on the atomic number of the target. For solid targets, the electron temperature is usually defined as a function of the normalized laser intensity ($I\lambda^2$), which is the product of the laser intensity, I(W/cm^2), and the square of the laser wavelength, λ(μm).

For normalized laser intensities in the range 10^{12} W/cm^{2}μm^2 $< I\lambda^2 <$ 10^{17} W/cm^{2}μm^2, Ref. [2] stated that inverse bremsstrahlung and resonance absorption are the dominant absorption mechanisms, with electron temperature expected to scale as $(I\lambda^2)^{1/3}$. An experimental result for the temperature scaling is described in Ref. [16], which gives

$$T \approx 6\times10^{-5}[I\lambda^2]^{\frac{1}{3}}. \quad (1)$$

Where T is the electron temperature in keV, I is the laser intensity in W/cm^2 and λ is the laser wavelength in m.

For very high normalized laser intensities, $I\lambda^2 > 10^{18}$ W/cm^{2}μm^2, relativistic J×B heating becomes the dominant absorption mechanism. The electron temperature can be estimated by Eq. (2), based on the ponderomotive force theory,

$$T = M_{\rm e}\times\left(-1.0+\sqrt{1.0+I\lambda^2/1.37\times10^{30}}\right). \quad (2)$$

Where $M_{\rm e}$ is the electron rest mass (0.511 MeV).

Reference [15] compares experimental results at the Rutherford Appleton Laboratory (RAL) Vulcan petawatt laser facility and the CallistoTi:sapphire laser at the Jupiter laser facility at LLNL with a calculation based on the ponderomotive theory. Even though the experimental results show electron temperature increasing as $(I\lambda^2)^{1/3}$, they were also observed to agree with the estimate using Eq. (2) (ponderomotive theory) within a factor of two for normalized laser intensities in the range 10^{18} W/cm^{2}μm^2 $< I\lambda^2 <$ 10^{20} W/cm^{2}μm^2.

Results for the electron temperature using Eq. (1) (Meyerhofer 1993), Eq. (2) (ponderomotive theory) and the experimental results summarized in [15] are shown in Fig. 1. Electron temperature estimates based on Eq. (1)

and (2) are observed to coincide when $I\lambda^2$=1.6×10^{17} W/cm^{2}μm^2. In this study, Eq. (1) was used to estimate the electron temperature when $I\lambda^2$ <1.6×10^{17} W/cm^{2}μm^2, while Eq. (2) was used when $I\lambda^2\geqslant$1.6×10^{17} W/cm^{2}μm^2.

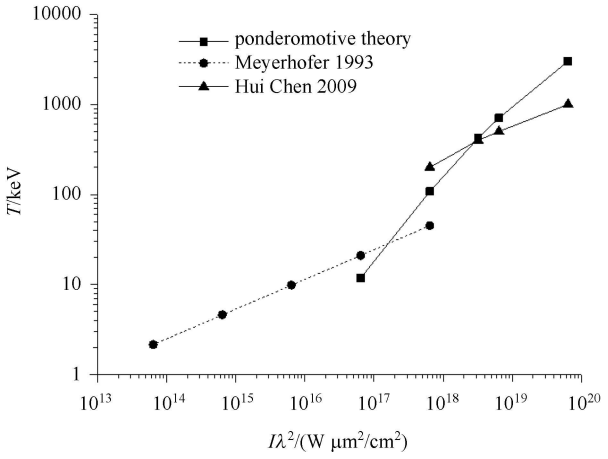

Fig. 1. Electron temperature, T, as a function of $I\lambda^2$.

2.3 Electron angular distribution

Reference [17] measured the angular distributions of hot electrons with very thin thermoluminescent dosimeters with a resolution of 10 degrees for 45° incidence onto a target at laser intensities of 10^{18}–10^{20} W/cm^2. At an intensity of 8×10^{17} W/cm^2, most of the hot electrons are at lower energies and the electron dose rate peaks at the front side of the target, likely due to target self-shielding. At an intensity of 2×10^{19} W/cm^2, the dose rate component behind the target increases. As the intensity reaches 8×10^{19} W/cm^2, the hot electrons are more energetic and the electron dose rate peaks at the far side of the target, with additional peaks in the laser direction.

These results show that the angular distribution of hot electrons is not isotropic (but not very anisotropic either) due to the energy distribution of hot electrons and the target self-shielding. In this study, the X-ray source was assumed to be isotropic.

2.4 X-ray spectrum

Studies have shown that the bremsstrahlung X-ray spectrum can be expressed as [3]:

$$N_{\rm p}(E_{\rm p})=C\frac{1}{R_{\rm p}}\exp\left(\frac{E_{\rm p}}{T}\right). \quad (3)$$

Where $E_{\rm p}$ is the photon energy, T is the electron temperature and C is a constant.

C is a constant which satisfies the condition that the integration of the energy of all the photons equals the product of the laser pulse energy and the laser energy to X-ray energy conversion efficiency. Therefore, C is dependent on the electron temperature, the laser pulse energy and the laser to X-ray energy conversion efficiency. The laser to X-ray energy conversion efficiency is determined by two processes: conversion of laser energy to the energy of hot electrons; and conversion of the energy of hot electrons to bremsstrahlung. Note that isotropic emission of the X-ray is assumed in the formula.

This X-ray spectrum formula is consistent with the electron spectra described in Section 2.2, when a bremsstrahlung yield spectrum of $E_{\rm p}^{-1}$ or $E_{\rm p}^{-2}$ is used. M. H. Key et al. also mention that a Maxwellian electron energy distribution gives an $e^{-E_{\rm p}/T}$ spectral shape for the bremsstrahlung [9]. Therefore, Eq. (3) was used to describe the X-ray source spectrum in the shielding attenuation calculations in Section 4.

3 X-ray dose

As Eq. (4) shows, Y. Hayashi et al. derived an equation to estimate the 0° photon dose generated from the interaction of a short pulse high power laser and a solid target [7]

$$\begin{aligned} &H_{\rm x}\approx 6.0\times10^5\times(P_{\rm ef.}/R^2)\times T(T\geqslant 3\ {\rm MeV}).\\ &H_{\rm x}\approx 2.0\times10^5\times(P_{\rm ef.}/R^2)\times T^2(T<3\ {\rm MeV}). \end{aligned} \quad (4)$$

Where $H_{\rm x}$ is the photon dose in mrem/J, $P_{\rm ef.}$ is the laser energy to electron energy conversion efficiency, R is the distance from the target to the measurement point in cm, and T is the hot electron temperature in MeV.

The equation was based on an electron spectrum with the relativistic Maxwellian distribution and the 0° bremsstrahlung dose formula proposed by Swanson [18] for estimating the forward dose of photons. A constant was applied to correct for the difference between the above analytic estimation and the EGS4 Monte Carlo calculations.

It can be found that photon dose is assumed to be proportional to the laser pulse energy in this equation. This is reasonable, as the number of hot electrons is proportional to the laser pulse energy under the above assumption for the electron energy distribution.

In practice, the parameters, which are usually well-known for any given laser facility, are the laser wavelength and laser intensity, rather than the laser energy to electron energy conversion efficiency and the electron temperature. Therefore, an estimation of X-ray dose at different laser intensities will be very useful for radiation protection studies at the laser facilities.

Using Eq. (4) and the electron source term (the-laser to-electron energy conversion efficiency and the electron temperature at different laser intensities) discussed in Section 2, the X-ray dose at different laser intensities can be calculated.

Figure 2 shows the X-ray dose at a distance of 1 m, calculated and plotted as a function of the normalized laser intensity ($I\lambda^2$) (line with circular points). In this calculation, as mentioned before, a laser-to-electron energy conversion efficiency of 30% for laser intensity below 10^{19} W/cm^2 and 50% above 10^{19} W/cm^2 was used. Eq. (1) was used to estimate the electron temperature for $I\lambda^2 < 1.6\times10^{17}$ W/cm^{2}μm^2, while Eq. (2) was used to estimate the electron temperature for $I\lambda^2 \geqslant 1.6\times10^{17}$ W/cm^{2}μm^2.

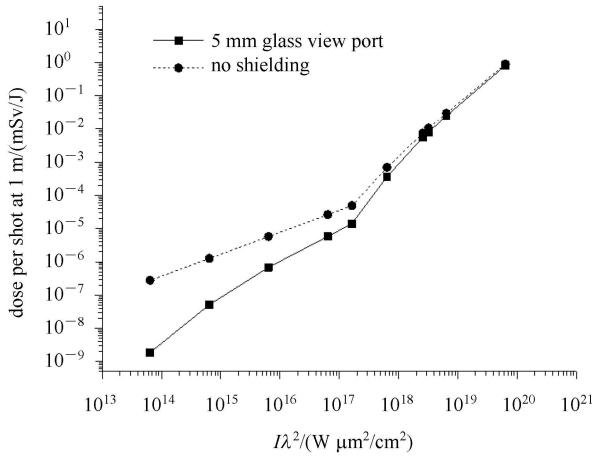

Fig. 2. X-ray dose per shot at 1 m with and without 5 mm glass view port shielding.

4 Shielding calculation

4.1 Shielding effects of the glass view port

Because the radiation hazard comes from a laser-target interaction in a vacuum, the vaccum chamber is the primary shielding item for the X-rays generated. Compared to the chamber wall, which is usually made from aluminum or stainless steel, the glass view port provides the least shielding for the laser induced X-rays. In this work, a 5-mm-thick glass view port for the target chamber was used to calculate the minimum shielding effect. The material of the glass was assumed to be borosilicate (Pyrex) with a density of 2.23 g/cm^3.

Calculations using the FLUKA Monte Carlo code [19] were conducted to estimate the shielding attenuation for X-ray spectra at various electron temperatures. Eq. (3) was used to describe the X-ray source spectrum and a FLUKA source routine was written to sample the photon energy from Eq. (3). The attenuation factor of 5-mm-thick glass shielding for ambient dose equivalent was calculated at different laser intensities.

The X-ray doses with and without the 5-mm-thick glass shielding are summarized in Fig. 2. It shows that, at low intensities, the attenuation from 5 mm glass is largely due to the low electron temperatures. When the laser intensity gets higher, the attenuation becomes less because the electron temperature gets higher and then the X-ray spectrum becomes harder and more difficult to attenuate.

Figures 3–5 show a comparison of the X-ray spectrum with and without 5 mm glass view port shielding at three electron temperatures: 4.6, 10 and 108 keV (corresponding to three intensities: 10^{15}, 10^{16} and 10^{18} W/cm^2). As the X-ray spectrum is different for these three intensities, the shielding effect of the 5-mm-thick glass is also different. The 5-mm-thick glass gave a higher attenuation for X-rays at the electron temperature of 4.6 keV (i.e., at the laser intensity of 10^{15} W/cm^2), which is consistent with the dose attenuation curve shown in Fig. 2. From Fig. 3 it can also be found that the 5-mm-thick glass does not provide any shielding effect for photons with energies higher than 50 keV.

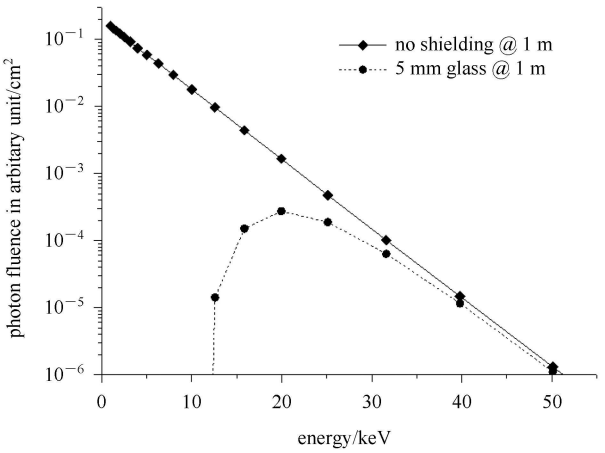

Fig. 3. X-ray spectrum with and without 5 mm glass view port shielding at T=4.6 keV.

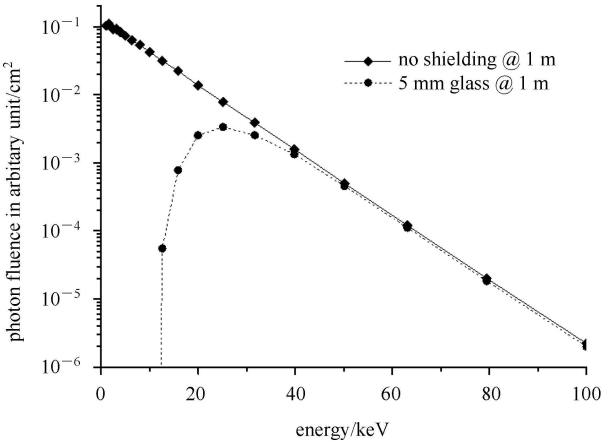

Fig. 4. X-ray spectrum with and without 5 mm glass view port shielding at T=10 keV.

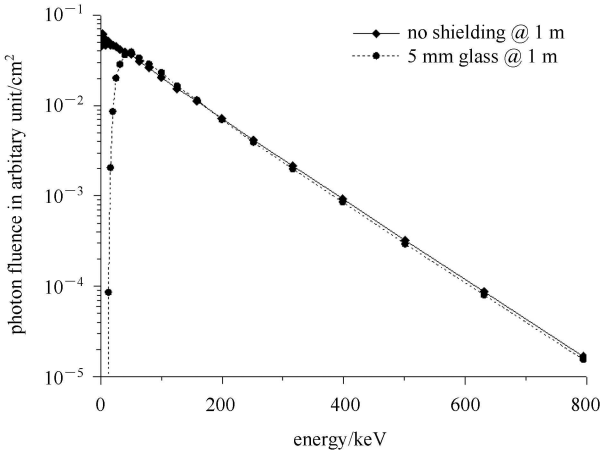

Fig. 5. X-ray spectrum with and without 5 mm glass view port shielding at T=108 keV.

4.2 Shielding calculation for typical shielding materials

In order to calculate the shielding thickness required to attenuate high-energy X-rays, general shielding calculations, including the transmission curves (ambient dose equivalent attenuation factors as a function of the shielding thickness) and the associated Tenth Value Layer (TVL) values, were performed with FLUKA. The shielding calculations were conducted for common shielding materials such as concrete (density of 2.35 g/cm^3), aluminum, stainless steel and lead.

To maximize the FLUKA calculation efficiency, the shielding layers were represented as concentric spherical shells at a distance of ∼5 m from the center, and the X-ray source was assumed to be isotropic and located at the center of the spheres. Two typical electron temperatures (400 and 1000 keV) were used and the results were compared under the two electron temperatures to find the influence of this parameter.

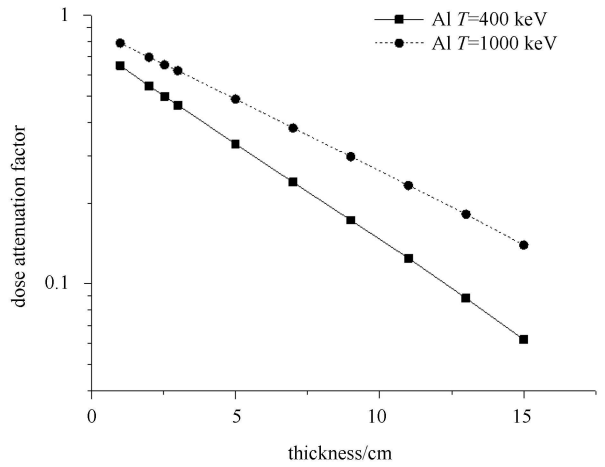

Fig. 6. Transmission curves of the equivalent ambient dose in aluminum.

Figures 6–9 show the calculated transmission curves of the equivalent ambient dose in concrete, aluminum stainless steel and lead at two electron temperatures (400 keV and 1000 keV), which give the dose attenuation factor as a function of the thickness.

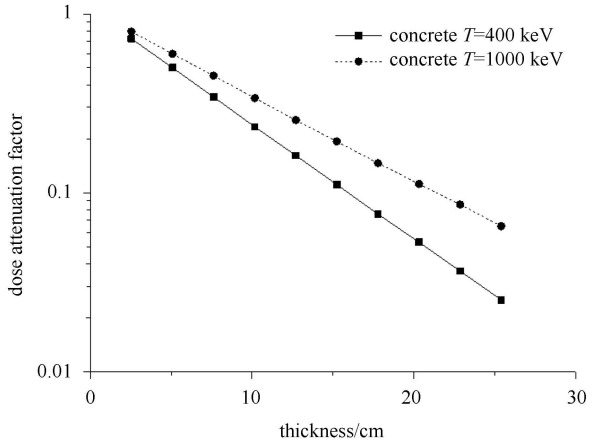

Fig. 7. Transmission curves of the equivalent ambient dose in concrete.

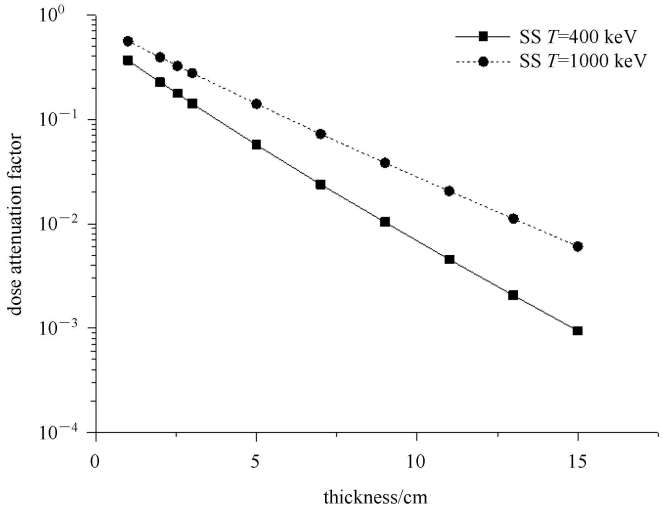

Fig. 8. Transmission curves of the equivalent ambient dose in stainless steel.

The TVL represents the thickness of a specified substance which, when introduced into the path of a given beam of radiation, reduces the dose rate by one tenth. The first TVL (TVL1) and the second TVL (TVL2) of each material for the X-ray source at two electron temperatures (400 keV and 1000 keV) were derived from the above dose transmission curves and are listed in Table 1. Generally the second TVL is larger than the first TVL because the photon spectrum becomes harder when the lower-energy photons are preferentially removed. These data will be useful for the shielding design of high intensity laser facilities.

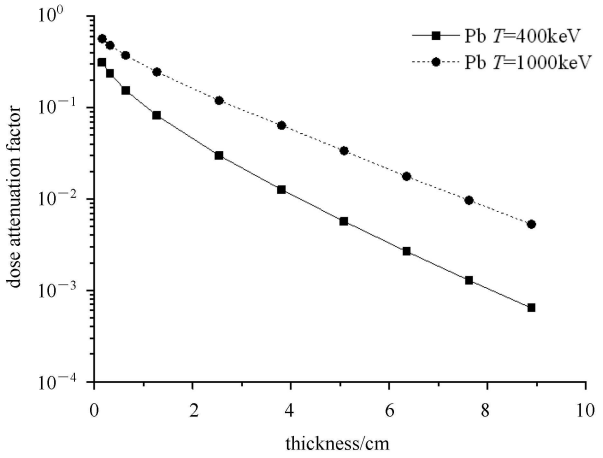

Fig. 9. Transmission curves of ambient dose equivalent in lead.

Table 1. The first TVL (TVL1) and the second TVL (TVL2) of different materials for X-rays at two electron temperatures.

material	T=400 keV		T=1000 keV	
	TVL1/cm	TVL2/cm	TVL1/cm	TVL2/cm
concrete	15.7	16	21.1	21.3
lead	1	3.2	2.8	4.8
SS	3.9	5.4	6.2	7.2
AL	12.2	26.1	17.8	36.5

5 Summary

Ionizing radiation induced by the laser-target interaction has become a new radiation hazard at high intensity laser facilities. Bremsstrahlung X-rays caused by the hot electrons can generate significant amounts of dose.

In this paper, we have reviewed the available literature on the physics and characteristics of laser-induced hot electrons and X-ray hazards. Several important aspects were analyzed, including the laser-to-electron energy conversion efficiency, electron angular distribution, electron energy spectrum and effective temperature, and bremsstrahlung production of X-rays in the target.

Based on this information, the X-ray dose generated with high-Z targets for laser intensities between 10^{14} and 10^{20} W/cm^2 was estimated. The results show that the X-ray dose at 1 m from a solid target can be estimated to be 2.6×10^{-5}, 6.9×10^{-4}, 0.03 and 0.9 mSv/J at 10^{17}, 10^{18}, 10^{19} and 10^{20} W/cm^2, respectively. This curve (photon dose vs. laser intensity) provides a straightforward tool to estimate the X-ray dose in practice, as the laser intensity is a well-known parameter for laser facilities.

The shielding effects of common shielding items such as the glass view port, aluminum chamber wall and concrete wall were also studied using FLUKA. The X-ray dose outside the 5 mm glass view port was calculated and compared to that without any shielding. The transmission curves and the associated Tenth Value Layer (TVL) values were calculated for concrete, aluminum, stainless steel, and lead. This work provides useful information for the radiation safety design of high intensity laser facilities.

We would like to express our appreciation to Greg Hays, HaeJa Lee, Richard M. Boyce and Bob Nagler (SLAC) for their useful discussions; and Hui Chen and Scott Wilks (LLNL) for providing information about the electron temperature study results.

References

1 Wilks S C, Kruer WL. IEEE J. Quantum Elect, 1997, **33**: 1954
2 Baldis H A, Campbell E M, Kruer W L. Handbook of Plasma Physics. Elsevier Science Publishers, 1991, 156–182
3 CHEN L M, Forget P, Fourmaux S et al. Phys. Plasmas, 2004, **11**: 4439
4 GUO T, Spielmann C, Walker B C et al. Rev. Sci. Instr., 2001, **72**: 41
5 Borne F, Delacroix D, Gelé J M et al. Radiat. Prot., Dosim., 2002, **102**(1): 61
6 Clarke R J, Neely D, Edwards R D. Radiol. Prot., 2006, **26**: 277
7 Hayashi Y, Fukumi A, Matsukado K et al. Radiat. Prot. Dosim., 2006, **121**(2): 99
8 Hatchett S P, Brown C G, Cowan T E et al. Phys. Plasmas, 2000, **7**(5): 2076
9 Key M H, Cable M D, Cowan T E et al. Phys. Plasmas, 1998, **5**(5): 1966
10 Myatt J, Theobald W, Delettrez J A et al. Phys. Plasmas, 2006, **13**: 043102
11 Hesham K, Sandra B. Nucl. Technol, 2009, **168**: 381
12 Hatchett S P, Brown C G, Cowan T E et al. Phys. Plasmas, 2000, **7**: 2076
13 Perry M D, Sefcik J, Cowan T et al. Laser Driven Radiography, LLNL- UCRL-ID-129314, 1997
14 Ledingham K W D, Spencer I, McCanny T et al. Phys. Rev. Lett., 2000, **84**(5): 899
15 CHEN H, WilksS C, Kruer W L et al. Phys. Plasmas, 2009, **16**(2): 020705
16 Meyerhofer D D, CHEN H, Delettrez J A et al. Phys. Fluids B, 1993, **5**: 2584
17 PING Y, Shepherd R, Lasinski B F et al. Phys. Rev. Lett., 2008, **100**(8): 085004
18 Swanson W P. IAEA Technical Report Series 188, 1979. 53
19 Fassò A, FerrariA,Ranft J et al. FLUKA a Multi-particle Transport Code. CERN-2005-10, INFN/TC_05/11, SLAC-R773.2005